

https://doi.org/10.1070/QEL16983

Dual-wavelength generation of picosecond pulses with 9.8 GHz repetition rate in Nd : YAG waveguide laser with graphene

M.V. Ponarina, A.G. Okhrimchuk, M.G. Rybin, M.P. Smayev, E.D. Obraztsova, A.V. Smirnov, I.V. Zhluktova, V.A. Kamynin, T.V. Dolmatov, V.V. Bukin, P.A. Obraztsov

Abstract. **We report a new solid-state waveguide laser generating picosecond pulses with a GHz repetition rate, based on the use of graphene as a saturable absorber. Lasing at the main transverse mode is provided by the geometry of a cylindrical waveguide formed in the active crystal volume by the method of direct writing with a femtosecond laser beam. Fine tuning of the intracavity interferometer formed between the active medium and output mirror makes it possible to control the spectral-temporal parameters of output radiation and to smoothly tune the repetition rate of pulses having a duration of less than 20 ps. In particular, the possibility of dual-wavelength generation in the regime of continuous passive mode locking using a single saturable absorber based on graphene is demonstrated. By amplifying laser output radiation in the ytterbium fibre amplifier, an average output power of 530 mW is obtained.**

Keywords: *waveguide lasers, ultrashort pulses, gigahertz pulse repetition rate, Nd : YAG, mode locking, graphene, direct laser writing.*

1. Introduction

Due to a high rate of the development of technologies and information society, the need for a fast transfer of large amounts of information is constantly increasing. One of the possible ways to speed up the information transfer is the use of laser sources with a pulse repetition rate of more than 1 GHz, optical radiation spectrum of which represents a set of equidistant lines [1].

There are various approaches to the development of highly stable laser pulse emitters, based on the use of both bulk solid-state or semiconductor lasers with a short (micro) resonator, and fibre lasers operating in the regime of fundamental or harmonic mode locking [2, 3]. Harmonic mode locking is understood as a laser operation regime in which several pulses with equal time intervals exist in the resonator simultaneously [4]. However, one of the simplest and most compact systems is a laser, the resonator of which consists of two plane-parallel mirrors, partially or completely filled with an active medium (a glass or a crystal doped with rare-earth ions).

One of the main conditions for achieving stable mode locking is the operation in the fundamental transverse mode (TEM_{00}). Reaching the single-mode regime is often complicated by the appearance of thermal effects in crystals, the contribution of which increases with pump intensity. For example, under high-power pumping, the refractive index in a crystal is distributed inhomogeneously, which leads to lasing on several transverse modes [5]. To eliminate such effects, it is proposed in the present work to use a waveguide structure formed inside the active crystal. The use of the waveguide geometry provides the effective input and uniform propagation (without divergence) of optical pump radiation along the entire length of the active element. The small size of cylindrical waveguides, corresponding to the TEM_{00}-mode diameter, allows single-mode lasing to be attained.

Saturable absorbers such as semiconductor saturable absorber mirrors (SESAMs) [6, 7], and in recent years carbon nanotubes [8, 9] and graphene [10–12], are traditionally used for passively mode-locked laser operation. Compared to other saturable absorbers, graphene has a number of advantages: small thickness, ultrafast (less than 5 ps) relaxation times, constant linear transmittance ($\sim 2\%$) in the UV-to-IR range, and a possibility for direct application to the active element or the resonator mirror [13].

Thus, the aim of this work is to implement a continuous regime of passive mode locking in a compact Nd:YAG waveguide laser with gigahertz pulse repetition rate by means of a saturable graphene-based absorber.

2. Experimental

A schematic of a passively mode-locked, solid-state, graphene-based Nd:YAG waveguide laser is shown in Fig. 1. To pump the active element, radiation from a cw Ti : sapphire laser with a centre wavelength of 808 nm and an average power of 600 mW was used. Pump radiation was focused onto a waveguide structure formed inside an Nd (1 at.%) : YAG crystal

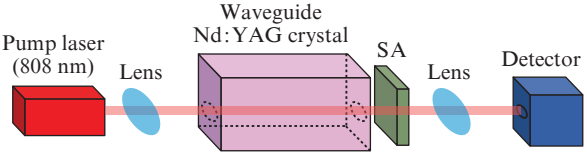

Figure 1. Experimental scheme of the Nd: YAG waveguide laser.

M.V. Ponarina, M.G. Rybin, E.D. Obraztsova, A.V. Smirnov, I.V. Zhluktova, V.A. Kamynin, T.V. Dolmatov, V.V. Bukin, P.A. Obraztsov A.M. Prokhorov General Physics Institute, Russian Academy of Sciences, ul. Vavilova 38, 119991 Moscow, Russia, e-mail: ponarinamariya@gmail.com, p.obraztsov@gmail.com;
A.G. Okhrimchuk Fiber Optics Research Center, Russian Academy of Sciences, ul. Vavilova 38, 119991 Moscow, Russia; D. Mendeleev University of Chemical Technology of Russia, pl. Miusskaya 9, 125047 Moscow, Russia;
M.P. Smayev D. Mendeleev University of Chemical Technology of Russia, pl. Miusskaya 9, 125047 Moscow, Russia

Received 27 February 2019
Kvantovaya Elektronika **49** (4) 365–370 (2019)
Translated by M.A. Monastyrskiy

using the method of direct writing with a femtosecond laser beam [14]. A cylindrical-type waveguide with a cladding having a reduced refractive index and a core diameter of 30 μm was written by a beam of a femtosecond 'generator–regenerative amplifier' laser system emitting pulses with a duration of 180 fs at a wavelength of 1030 nm. The laser beam was focused in the Nd:YAG crystal volume at a depth of about 200 μm by a lens with a numerical aperture NA = 0.65 and a cylindrical lens with a focal length of f = –400 mm placed directly in front of the lens along the beam. Thus, an astigmatic beam was formed behind the lens, with two elliptical waists in the beam cross section and a ratio of the major and minor ellipse axes about 10. The sample was placed onto an Aerotech precision three-coordinate translation stage and was scanned relative to the beam waist, with the result that a trace (track) of the refractive index reduced by a value of 5×10^{-3} was left in the sample. The beam waist closest to the lens was used for writing. The major axis of elliptical waist was oriented along the scan, i.e. parallel to the track being written. To form the waveguide cladding, as many as 32 parallel tracks located along the cylinder generatrix were written, the core remaining non-irradiated.

A plane-parallel resonator of the Nd:YAG laser is formed by two mirrors: a dichroic mirror (highly reflecting in the range of 1060–1070 nm and transparent at a pump wavelength of 808 nm) deposited onto the crystal's input end-face, and an output mirror with a reflection coefficient of 98% at a wavelength of 1064 nm. Passive mode locking was provided by a saturable absorber (SA) based on graphene deposited directly onto the resonator output mirror. For precise control of the resonator length, the graphene-based output mirror was equipped with a piezoelectric element.

For the manufacture of a saturable absorber, a monatomic layer of carbon (graphene) [15] was synthesised using chemical vapour deposition (CVD) on a copper foil with subsequent etching and deposition onto the output mirror [16]. The external view of the output mirror with a deposited graphene-based saturable absorber is shown in Fig. 2d.

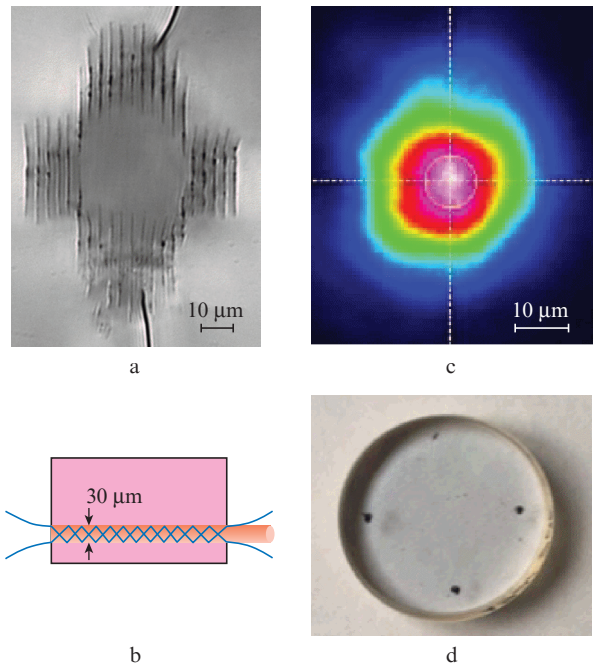

Figure 2. (a) Microphotograph of the waveguide, (b) scheme of pump radiation propagation inside the waveguide, (c) beam profile demonstrating the radiation mode composition in the waveguide, and (d) photograph of the resonator's output mirror with deposited graphene.

3. Results and discussion

The pulse repetition rate during laser operation in the regime of passive mode locking is determined by the double round-trip transit time for the radiation in the resonator. Thus, the resonator with a length of ~8.4 mm provides a pulse repetition rate of ~9.8 GHz, and its fine tuning in the range of 2 μm by means of a piezoelectric element provides frequency tuning with accuracy up to units of MHz.

Figure 3 displays a typical output radiation oscillogram measured using a photodiode (DILAZ DFDSH 40-16, 16 GHz bandwidth) and an oscilloscope (Tektronix DPO 71604C, 16 GHz bandwidth), as well as radiofrequency and optical spectra of the Nd:YAG waveguide laser, measured using optical (ANDO AQ6317B, 0.01 nm resolution) and radiofrequency (Agilent N9020A, 2 Hz resolution) spectrum analysers, respectively. The average output power constituted 1 mW, which is due to the use of the output resonator mirror with a reflectance of 98%. In experiments, a PS-1/S1 electron-optical camera with a time resolution of 1 ps was used in real-time regime to measure the duration of individual generated pulses and to provide additional diagnostics of the resulting pulse comb [17]. The pulse duration was less than 20 ps. A detailed description of the technique for pulse duration measurement and the diagnostics of output radiation is given in [13, 18].

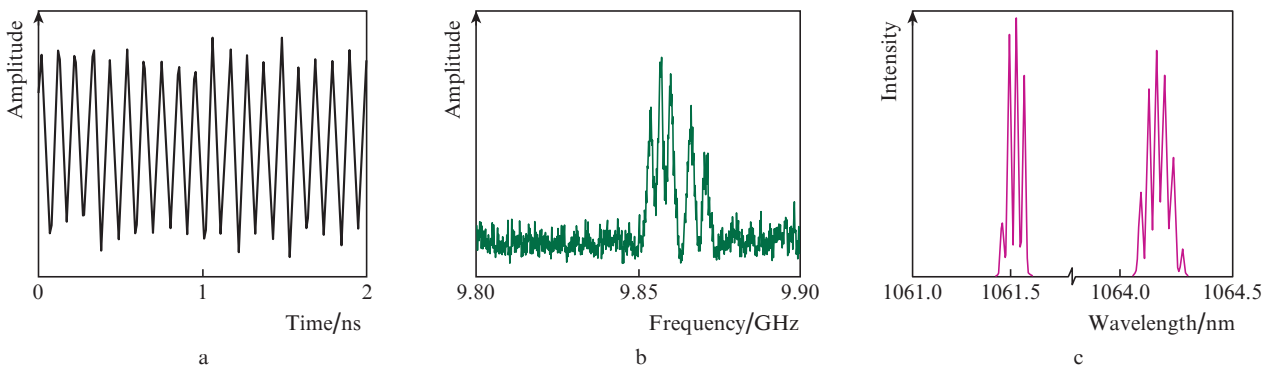

Figure 3. (a) Oscillogram of laser output, and (b) radiofrequency and (c) optical spectra.

The laser power modulation observed in Fig. 3a leads to the appearance of additional lines in the radiofrequency spectrum of output radiation (Fig. 3b). In this case, as can be seen from Fig. 3c, there are two groups of lines in the optical spectrum, with maxima at 1061.58 and 1064.18 nm, consisting of distinctly different longitudinal modes. It should be noted that similar types of oscillograms and radiation spectra were observed at different resonator lengths; herewith, precise adjustment of the output mirror position by means of a piezoelectric element did not allow one to obtain a single spectral component in the radiofrequency spectrum in the vicinity of 10 GHz.

In the Nd:YAG crystal, in the region of 1 μm there are several energy transitions corresponding to wavelengths of 1061.58 (9420), 1064.18 (9397), and 1064.55 nm (9394 cm^{-1}) [19]. The experimentally obtained output radiation spectrum corresponds to the generation of Nd^{3+} ion at transitions from the R_1 and R_2 sublevels of the $^4F_{3/2}$ energy level to the split $^4I_{11/2}$ level. To study these transitions in the Nd:YAG crystal, the crystal's luminescence spectrum was measured using an OceanOptics USB4000 NIR spectrometer with a spectral resolution of 1 nm (Fig. 4).

One can see from Fig. 4 that the luminescence peak intensities for these laser transitions are different. The cross section of the $R_2 \rightarrow Y_3$ transition at a wavelength of 1064.18 nm is $\sigma_{1064.18} = 45.8\times10^{-20}$ cm^2. The transition to λ = 1061.58 nm ($\sigma_{1061.58} = 22.8\times10^{-20}$ cm^2) has a common R_1 upper level with a transition to λ = 1064.55 nm ($\sigma_{1064.55} = 8.1\times10^{-20}$ cm^2) [20]. To satisfy lasing conditions at several laser transitions in the Nd:YAG laser, it is necessary to use a resonator design providing spectral dependence of intracavity losses. In order to synchronise the radiation modes generated at several transitions, i.e., to ensure the same pulse repetition rate at different wavelengths, it is necessary that the total round-trip transit time in the resonator be the same.

In the laser scheme we used, the air gap formed between the uncoated end-face of the active crystal and the output mirror represents an intracavity interferometer (Fig. 5). The interferometer is a dispersion element which introduces a time delay of radiation propagation, dependent on the wavelength. Thus, depending on the interferometer length, a periodic change in the spectral and temporal characteristics of the output radiation should be observed.

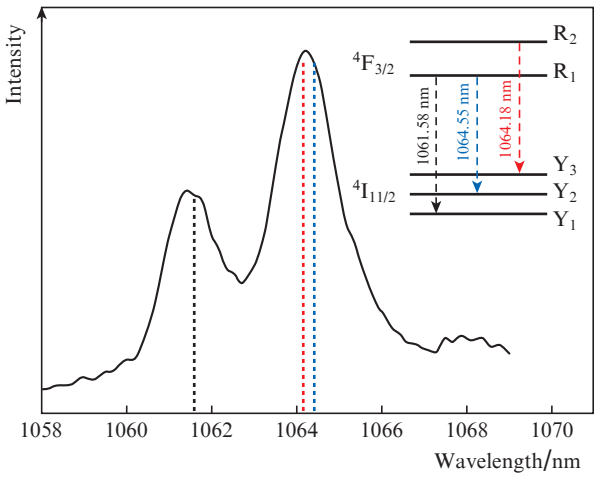

Figure 4. Luminescence spectrum of the Nd:YAG crystal and energy level diagram of transitions corresponding to wavelengths of 1061.58, 1064.18, and 1064.55 nm.

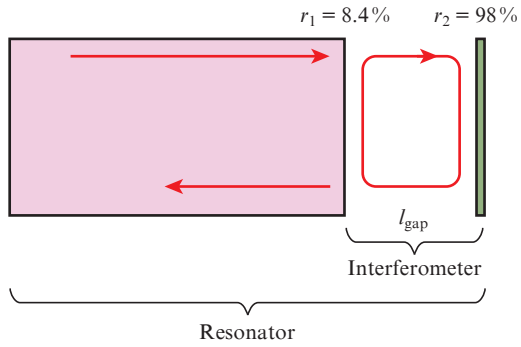

Figure 5. Schematic of the Nd:YAG waveguide laser resonator with an air interferometer.

As already noted, the resonator length adjustment by a piezoelectric element does not provide the same pulse repetition rate at different wavelengths. Therefore, to separate out radiation on one of the lasing lines (1061 or 1064 nm, see Fig. 3c), it was proposed to install an optical filter (OF-LINK TOF-1064) outside the resonator, tunable in a wavelength range of 1040–1080 nm and having a bandwidth of 1 nm and an input fibre diameter of 6 μm.

Figure 6 presents an oscillogram and also radiofrequency and optical spectra of the output laser radiation filtered at λ = 1061 nm. As follows from this Figure, after passing

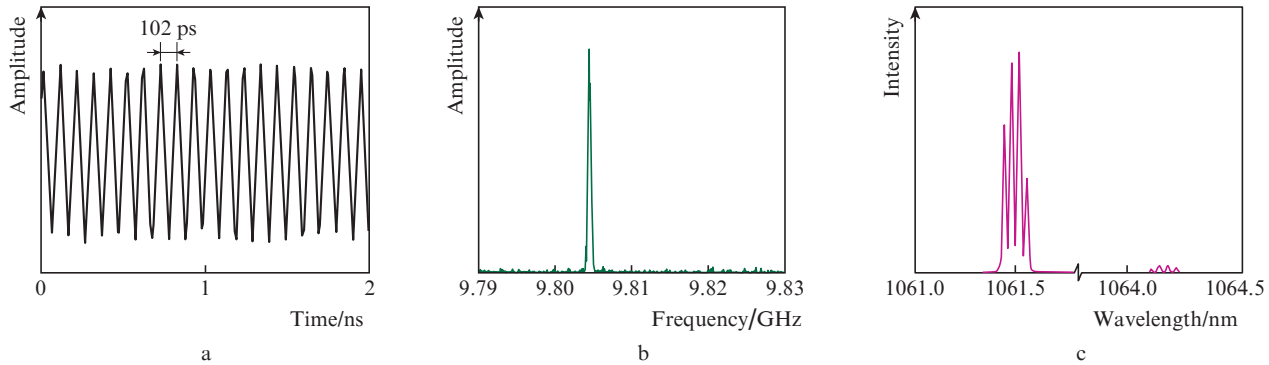

Figure 6. (a) Oscillogram of laser output after passing through the optical filter, and (b) its radiofrequency and (c) optical spectra.

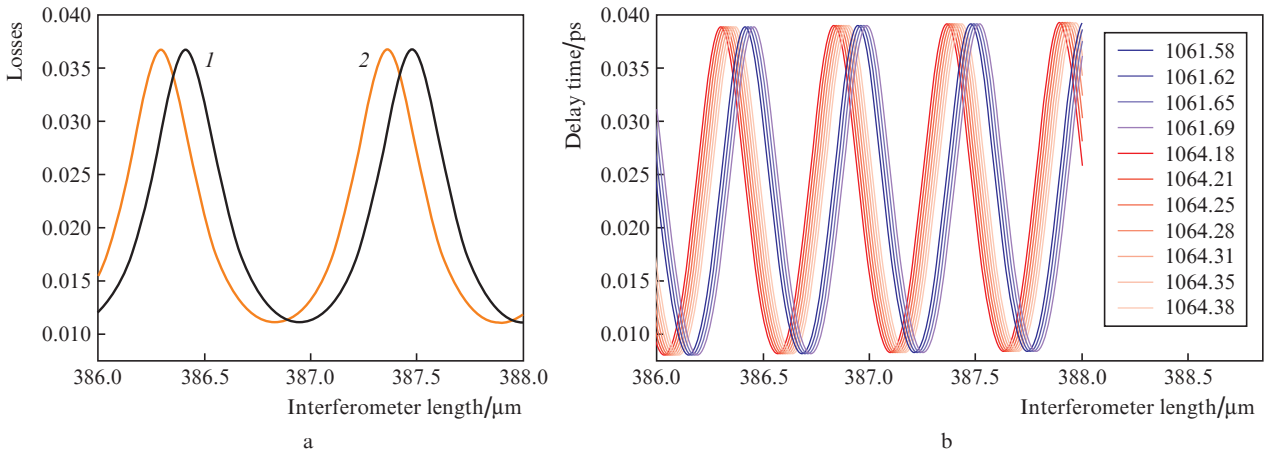

Figure 7. (Colour online) Calculated dependences of (a) intracavity losses and (b) time delay introduced by the interferometer for longitudinal modes at wavelengths of (*1*) 1061 and (*2*) 1064 nm on the interferometer length in the range 386–388 μm.

through the optical filter, the pulses propagate with a repetition rate of ~102 ps, and the radio frequency spectrum contains only one component. Thus, the use of an extracavity selective element based on a single-mode optical fibre resulted in a sequence of ultrashort pulses with a repetition rate of 9.8 GHz.

Note that this Nd:YAG waveguide laser was used as a master oscillator for an Yb-doped fibre amplifier [21, 22]. The amplified signal power constituted 530 mW.

The characteristics of radiation separated out at a wavelength of 1064 nm differ from those obtained at $\lambda = 1061$ nm. In this case, the radiofrequency intensity spectrum is similar to that shown in Fig. 3b and contains a set of non-equidistant lines apparently related to the incomplete mode locking.

To study the possible operation regimes of the developed waveguide laser, the intracavity interferometer parameters were calculated. The interferometer reflection coefficient is

$$R = 1 - \frac{(1-r_1)(1-r_2)}{(1-\sqrt{r_1 r_2})^2 + 4\sqrt{r_1 r_2}\,[\sin(\pi l_{\text{gap}}/\lambda)]^2}, \qquad (1)$$

where $r_1 = 8.44\%$ is the reflection coefficient of the uncoated end-face of the Nd: YAG crystal; $r_2 = 98\%$ is the reflection coefficient of the output mirror; and l_{gap} is the interferometer length.

The dependence of logarithmic losses $g_{\text{los}} = -\ln R$ on l_{gap} for wavelengths 1061 and 1064 nm is shown in Fig. 7a. To fulfil the dual-wavelength lasing condition, it is necessary that the losses introduced by the interferometer at a wavelength of 1064 nm exceed those at $\lambda = 1061$ nm. As can be seen from the periodic dependence $g_{\text{los}}(l_{\text{gap}})$ obtained, there are regions in which lasing at two wavelengths is possible.

The group velocity dispersion caused by the interferometer is [23]

$$\text{GDD} = 2\pi(2l_{\text{gap}}/c)^2 \frac{(r_1^2 - 1)2r_1 \sin(4\pi l_{\text{gap}}/\lambda)}{[1 - r_1^2 - 2r_1\cos(4\pi l_{\text{gap}}/\lambda)]^2}. \qquad (2)$$

The corresponding group delay caused by the interferometer appears as

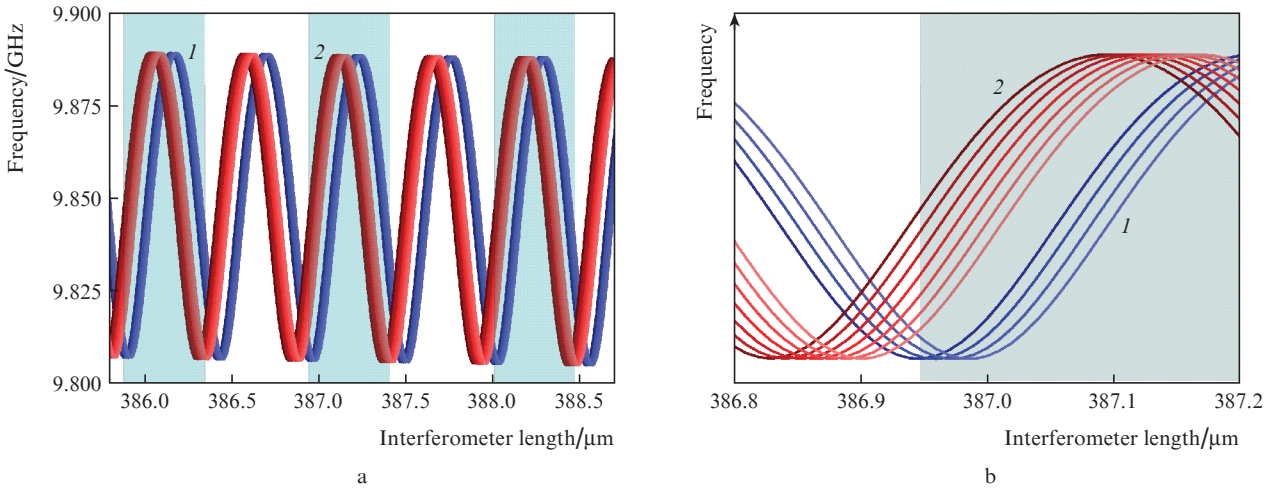

Figure 8. Dependences of the pulse repetition rate on the interferometer length with allowance for the distribution of longitudinal modes at wavelengths of (*1*) 1061 and (*2*) 1064 nm. Marked regions correspond to the interferometer lengths at which the intracavity losses at $\lambda = 1064$ nm exceed those at $\lambda = 1061$ nm.

$$\tau = (2l_{gap}/c)\frac{r_1^2 - 1}{r_1^2 - 1 + 2r_1\cos(4\pi l_{gap}/\lambda)}. \quad (3)$$

A periodic dependence of the group delay on the interferometer length, calculated for various longitudinal radiation modes in the vicinity of the wavelengths of 1061 and 1064 nm, is shown in Fig. 7b.

Based on the data obtained, the pulse repetition rate dependence was calculated with allowance for the distribution of longitudinal modes at wavelengths of 1061 and 1064 nm (Fig. 8), and also the range of interferometer lengths was selected to fulfil the condition of dual-wavelength lasing (for example, at l_{gap} in the region of 387 μm). At $l_{gap} \approx 387$ μm, the calculated time delay between modes at a wavelength of 1064 nm is approximately 50 fs, and at a wavelength of 1061 nm this delay is close to zero.

Figure 9 presents the radiofrequency spectrum obtained experimentally with separating out radiation at wavelengths of 1061 and 1064 nm and the calculated pulse repetition rate values at $l_{gap} = 386.97$ and 387.0 μm.

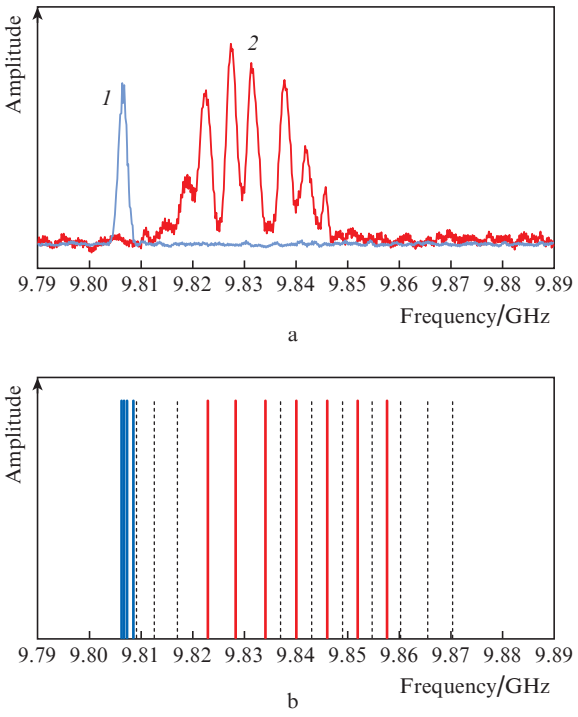

Figure 9. Comparison of the positions of the radiofrequency spectra' peaks (a) obtained in the experiment and (b) calculated for two positions of the output mirror for radiation at $\lambda = (1)$ 1061 and (2) 1064 nm. Solid lines indicate frequencies corresponding to $l_{gap} = 386.97$ μm, dotted lines show frequencies corresponding to 387.00 μm.

The pulse repetition rates calculated for the interferometer at $l_{gap} = 386.97$ μm are in good agreement with the radiofrequency spectrum obtained in the experiment. In this case, an increase in the interferometer length only by 0.03 μm leads to a significant change in the calculated frequencies. The coincidence of the calculated frequencies at a wavelength of 1061 nm ensures the fulfilment of the mode locking condition, which was actually observed in the experiment (see Fig. 6). In this case, the longitudinal modes at a wavelength of 1064 nm are not mode locked. Such a radiofrequency spectrum dependence is consistent with experimental data and qualitatively explains the laser regimes obtained and the possibility of their tuning.

4. Conclusions

Based on the waveguide in the Nd: YAG crystal and single-layer graphene, a solid-state picosecond laser with a pulse repetition rate of 9.8 GHz operating at wavelengths of 1061 and 1064 nm has been designed.

Controlling the losses and dispersion by means of adjusting the intracavity interferometer allows tuning the wavelength and pulse repetition rate, respectively. The possibility of coincidental dual-wavelength lasing in the regime of passive mode locking using a single graphene-based saturable absorber is demonstrated. This regime of laser operation may be of interest for the generation of terahertz radiation at a differential frequency of the wavelengths 1061.58 and 1064.18 nm ($\Delta\nu = 0.44$ THz).

Acknowledgements. P.A. Obraztsov expresses his gratitude to the Russian Science Foundation (Grant No. 17-72-103). The work of M.V. Ponarina, T.V. Dolmatov, and V.V. Bukin was supported by the the Presidium of the Russian Academy of Sciences (Basic Research Programme 'Extreme Light Fields and Their Interaction with Matter').

References

1. Hu H., Da Ros F., Pu M., Ye F., Ingerslev K., Porto E. *Nature Photon.*, **12**, 469 (2018).
2. Martinez A., Yamashita S. *Appl. Phys. Lett.*, **101**, 2012 (2012).
3. Chen H.-W., Chang G., Xu S., Yang Z., Kärtner F.X. *Opt. Lett.*, **37**, 3522 (2012).
4. Trikshev A.I., Kamynin V.A., Tsvetkov V.B., Itrin P.A. *Quantum Electron.*, **48**, 1109 (2018) [*Kvantovaya Elektron.*, **48**, 1109 (2018)].
5. Powell R.C., Payne S.A., Chase L.L., Wilke G.D. *Opt. Lett.*, **14**, 1204 (1989).
6. Mayer A.S., Phillips C.R., Keller U. *Nat. Commun.*, **8**, 1673 (2017).
7. Klenner A., Golling M., Keller U. *Opt. Express*, **22**, 11884 (2014).
8. Set S.Y., Yaguchi H., Tanaka Y., Jablonski M., Rozhin A. *Proc. 29th Eur. Conf. Opt. Commun. (ECOC'03)* (Rimini, 2003) paper PD44.
9. Choi S.Y., Calmano T., Rotermund F., Kränkel C. *Opt. Express*, **26**, 5140 (2018).
10. Sun Z., Hasan T., Torrisi F., Popa D., Privitera G., Wang F., Bonaccorso F., Basko D.M., Ferrari A.C. *ACS Nano*, **4**, 803 (2010).
11. Bao B.Q., Zhang H., Wang Y., Ni Z., Yan Y. *Adv. Funct. Mater.*, **19**, 3077 (2009).
12. Grivas C., Ismaeel R., Corbari C., Huang C.-C., Hewak D.W., Lagoudakis P., Brambilla G. *Laser Photon. Rev.*, **12**, 1800167 (2018).
13. Obraztsov P.A., Okhrimchuk A.G., Rybin M.G., Obraztsova E.D., Garnov S.V. *Laser Phys.*, **26**, 084008-1 (2016).
14. Okhrimchuk A., Mezentsev V., Shestakov A., Bennion I. *Opt. Express*, **20**, 3832 (2012).
15. Obraztsov P.A., Rybin M.G., Tyurnina A.V., Garnov S.V., Obraztsova E.D., Obraztsov A.N., Svirko Y.P. *Nano Lett.*, **11**, 1540 (2011).
16. Rybin M.G., Islamova V.R., Obraztsova E.A., Obraztsova E.D. *Appl. Phys. Lett.*, **112**, 2 (2018).
17. Garanin S.G., Bel'kov S.A., Rogozhnikov G.S., Rukavishnikov N.N., Romanov V.V., Voronich I.N., Vorob'ev N.S., Gornostaev P.B., Lozovoi V.I., Shchelev M.Ya. *Quantum Electron.*, **44**, 798 (2014) [*Kvantovaya Elektron.*, **44**, 798 (2014)].
18. Okhrimchuk A.G., Obraztsov P.A. *Sci. Rep.*, **5**, 11172 (2015).

19. Ievlev I.V., Koryukin I.V., Lebedeva Yu.S., Khandokhin P.A. *Quantum Electron*., **41**, 715 (2011) [*Kvantovaya Elektron*., **41**, 715 (2011)].
20. Demirbas U. *J. Opt. Soc. Am. B*, **35**, 2994 (2018).
21. Trikshev A.I., Kurkov A.S., Tsvetkov V.B. *Quantum Electron*., **42**, 417 (2012) [*Kvantovaya Elektron*., **42**, 417 (2012)].
22. Trikshev A.I., Kamynin V.A., Tsvetkov V.B., Egorova O.N. *Quantum Electron*., **46**, 1085 (2016) [*Kvantovaya Elektron*., **46**, 1085 (2016)].
23. Kafka J.D., Watts M.L., Pieterse J.-W.J. *IEEE J. Quantum Electron*., **28**, 2151 (1992).